Computer-aided detection of bladder tumors based on the thickness mapping of bladder wall in MR images

Hongbin Zhu[1], Chaijie Duan[1,3], Ruirui Jiang[2], Yi Fan[1], Xiaokang Yu[2], Wei Zeng[2], Xianfeng Gu[2] and Zhengrong Liang[1,2*]

Departments of Radiology[1] and Computer Science[2], Stony Brook University, Stony Brook, NY 11794
Beijing Key Lab of Medical Physics and Engineering[3], Institute of Heavy Ion Physics, Peking University, Beijing 100871, China

ABSTRACT

Bladder cancer is reported to be the fifth leading cause of cancer deaths in the United States. Recent advances in medical imaging technologies, such as magnetic resonance (MR) imaging, make virtual cystoscopy a potential alternative with advantages as being a safe and non-invasive method for evaluation of the entire bladder and detection of abnormalities. To help reducing the interpretation time and reading fatigue of the readers or radiologists, we introduce a computer-aided detection scheme based on the thickness mapping of the bladder wall since locally-thickened bladder wall often appears around tumors. In the thickness mapping method, the path used to measure the thickness can be determined without any ambiguity by tracing the gradient direction of the potential field between the inner and outer borders of the bladder wall. The thickness mapping of the three-dimensional inner border surface of the bladder is then flattened to a two-dimensional (2D) gray image with conformal mapping method. In the 2D flattened image, a blob detector is applied to detect the abnormalities, which are actually the thickened bladder wall indicating bladder lesions. Such scheme was tested on two MR datasets, one from a healthy volunteer and the other from a patient with a tumor. The result is preliminary, but very promising with 100% detection sensitivity at 7 FPs per case.

Keywords: Bladder tumor, magnetic resonance images, computer-aided detection, bladder wall, potential field, thickness mapping, conformal mapping, blob detection.

1. INTRODUCTION

According to American Cancer Society, bladder cancer is the fifth leading cause of cancer deaths in the United States, and early diagnosis of bladder abnormalities is crucial for effective treatment of bladder carcinoma [1, 2]. In addition, bladder cancer is reported to have high recurrence rate after resection of the tumors (as high as 80%) [3]. As the main method of investigating bladder abnormalities, fiber optic cystoscopy (OCys) [4] is accurate and can biopsy when tumor is found. But it is invasive, time-consuming, expensive, uncomfortable, incapable of viewing the entire bladder mucosa, and has the risk of urinary tract infection. Recently, computed tomography (CT)-based [5] and magnetic resonance (MR)-based [6] virtual cystoscopy (VCys) have been developed as an alternative means for bladder cancer detection and evaluation. Such methods are safe, less or non-invasive, and less expensive as compared to OCys. In CT or MR bladder images, it is expected that early sign of bladder lesion would be reflected by both the morphology and texture on the bladder wall and mucosa [6, 7]. Radiologists have to read the image slices one-by-one to locate possible abnormalities. Three-dimensional (3D) endoscopic views on the mucosa can be made available to assist the detection. Such reading process is time-consuming and brings fatigue error of diagnosis. Fortunately, computer-aided detection (CAD) of bladder tumors shows potential to be a second reader to help radiologists improving their performance. At early stages, flat and/or small tumors less than 5 mm are difficult to be detected and, therefore, deserved more attention [8]. Conventional characteristic features on the bladder wall, like curvedness and shape index, vary significantly from voxel to voxel [9]. In contrast, for a small bump protruding out of the bladder wall, the measurement of the thickness between the inner and outer borders tends to be a good indicator of the occurrence of abnormalities [10, 11]. In this study, the term "bladder wall" indicates the volumetric shell encompassed by the inner and outer borders. Therefore, we would like to introduce a CAD scheme of bladder tumors based on the features of the thickness mapping of the bladder wall in MR images.

* Correspondence: Z. Liang; Email: jerome.liang@sunysb.edu; Phone: (631) 444-7837; Fax: (631) 444-6450.

2. METHODS

2.1 Overview of the CAD scheme

Our algorithm is actually a two-stage process, i.e., bladder wall segmentation and tumor detection, as shown in Fig. 1. Starting from the T_1-weighted MR bladder images, a couple-level set segmentation method (as described in Section 2.2) is employed to retrieve the inner and outer bladder walls (the borders of the bladder shell). Based on the segmented bladder wall, the procedure of thickness mapping is conducted on the inner border with a thickness value assigned on each voxel of the inner border (detailed in Section 2.3). Bladder tumors with various sizes bulge into lumen area from the inner border in various shapes, like polypoid, sessile, abnormal plaques, and even flat. However, they share a common feature of being protrusions out of the bladder wall, which leads to a sudden change of bladder wall thickness. To simplify the problem, we flatten the 3D thickness mapping to a two dimensional (2D) gray image through using the conformal mapping method (as described in Section 2.4). Such abnormality can then be detected through using a 2D blob detector (detailed in Section 2.5) on the 2D flattened inner border.

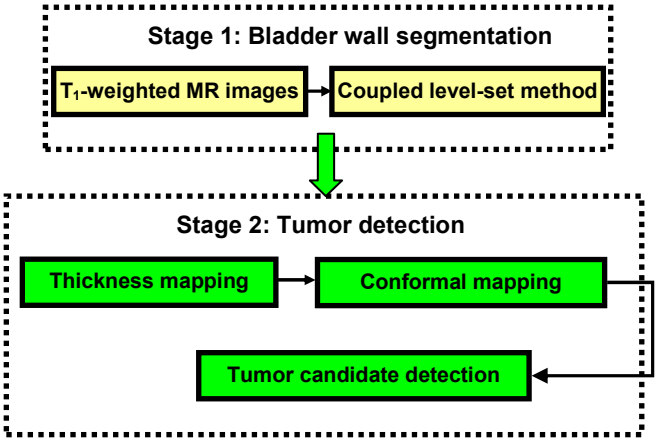

Fig. 1. The pipeline of the presented method.

2.2 Coupled level-set method

As opposed to T_2-weighted MR images (Fig. 2(a)), T_1-weighted MR images (Fig. 2(b)) lower the image intensities of urine for the contrast against the wall and have less partial volume effect at the inner border. In this study, we apply the coupled level set method to segment the inner and outer borders of the bladder wall from T_1-weighted MR images (Fig. 2(c)).

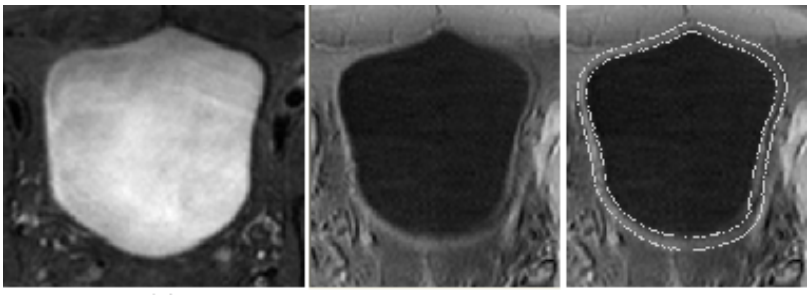

Fig. 2. (a) A typical T_2-weighted MR image slice of a bladder. (b) A typical T_1-weighted MR image slice of the same bladder as in (a). (c) The segmented inner and outer borders of the bladder wall (same slice as (b)).

By coupled level set, we refer to the collaboration between two level set functions, for automated delineation of bladder wall inner and outer borders, prior to the thickness mapping. By defining image and geometry energy functions, based on the modified Chan-Vese model [12] and the regional adaptive clustering algorithm, the coupled level set

algorithm is well adapted to T_1-weighted bladder MRI. The method significantly differs from most of the previous bladder segmentation work mainly from three aspects. First of all, the proposed level set-based segmentation pipeline automatically, rather than manually extracts the inner and outer borders of bladder wall. Secondly, T_1-weighted bladder MRI with decreased urine intensities, as opposed to CT and urine tagging in T_2-weighted scenario, becomes the major interest and based on which, the coupled level set algorithm is developed. Thirdly, by considering the global intensity distribution, as well as the local intensity contrast, the image energy function is capable of overcoming the inhomogeneity, non-uniformly scattered motion artifacts and image noise. More details can be found in [13].

2.3 Thickness mapping

The segmented inner and outer borders are spatially 3D surfaces. The term "thickness" here means the length of a path starting from a point on one surface and ending at another point on the other surface, and the path is constrained by the local shape of the two surfaces. As shown in Fig. 3(a), the desired path starting from point A would be the dashed line AB instead of AC. In our previous work [13], the two borders were assumed as two iso-potential surfaces which generated electric potential between them, and the integral path was traced along the gradient direction of the potential field, as shown in Fig. 3(b). However, the implementation of the idea was simplified based on the voxel units, and the computed value may not be accurate for CAD. In this study, we implement the idea based on a potential field inside the wall and explore a CAD scheme for bladder tumor detection based on the resulted thickness mapping.

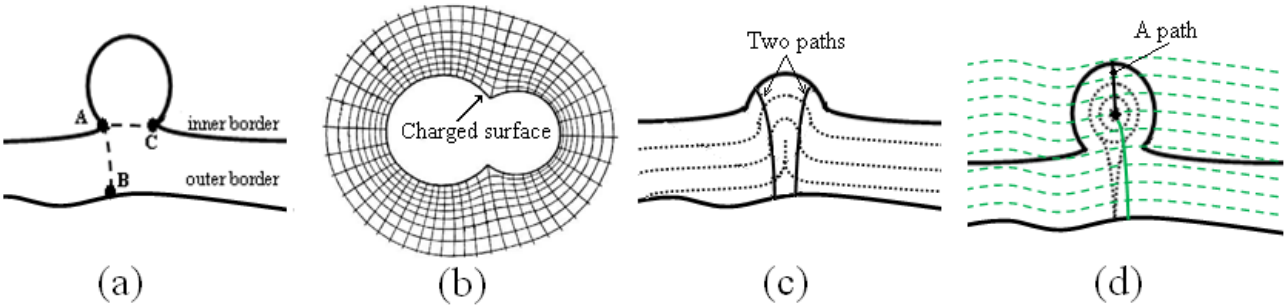

Fig. 3. (a) Paths used to measure the thickness between the inner and outer borders. (b) The potential field distribution. The inner-most solid curve denotes the original charged surface. The close thin curves represent the iso-potential surfaces of the generated potential field, and the radial thin curves indicate the electric field lines generated by the original charged surface. (c) The top/bottom thick curve represents the inner/outer border. The half-circle like bump on the inner border mimics a possible bladder lesion, like a sessile or flat small one. The thin dotted curves indicate the iso-distance surfaces of the distance transform (DT) based on the inner border. (d) With similar notations as (c), this is another case with a lesion bulging more into bladder lumen mimicking more advanced lesions. While the green dashed curves represent the other DT on the outer border.

The accurate computation of the electric potential between the two surfaces would be rather complicate and time consuming. We notice that the distance transform (DT) [14] based on the inner/outer border has similar properties as that of electric potential field. The iso-distance surfaces are smooth and not self-intersecting and there is only one path if we trace along the gradient direction of the DT. As shown in Fig. 3(b), the closed thin curves can also be assumed as the iso-distance surfaces of the DT based on the charged surface. Therefore, we utilize the DT to approximate the electric potential field. The fast marching method [15] can be used since we just need to know the DT inside the bladder wall. The dotted black curves in Fig. 3(c) and 3(d) represent the iso-distance surfaces based on the top thick black curves. In the method, starting from a point on the inner border, we trace along the gradient direction of the DT based on the inner border towards the outer border, and the tracing will stop if it reaches the outer border. As shown in Fig. 3(c), the two solid curves between the two borders are two paths traced along the gradient direction of the DT based on the inner border. However, things are not always that easy. As shown in Fig. 3(d), the black solid curve representing a path is traced from the inner border towards the outer border. But the tracing will stop at the center of the lesion since the DT converges there. Interestingly, such convergence actually indicates the abnormality. In our previous work [13], a predefined large value would be assigned to the starting point for such case. However, in this study, we would like to continue the tracing process further to reach the outer border by following the reverse direction of the gradient of the DT based on the outer border. As shown in Fig. 3(d), the green solid curve denotes the part of the path generated by the second tracing. Fig. 4 shows the resulted thickness mapping superimposed on the 3D bladder model of two cases, where the different colors indicate different thickness values.

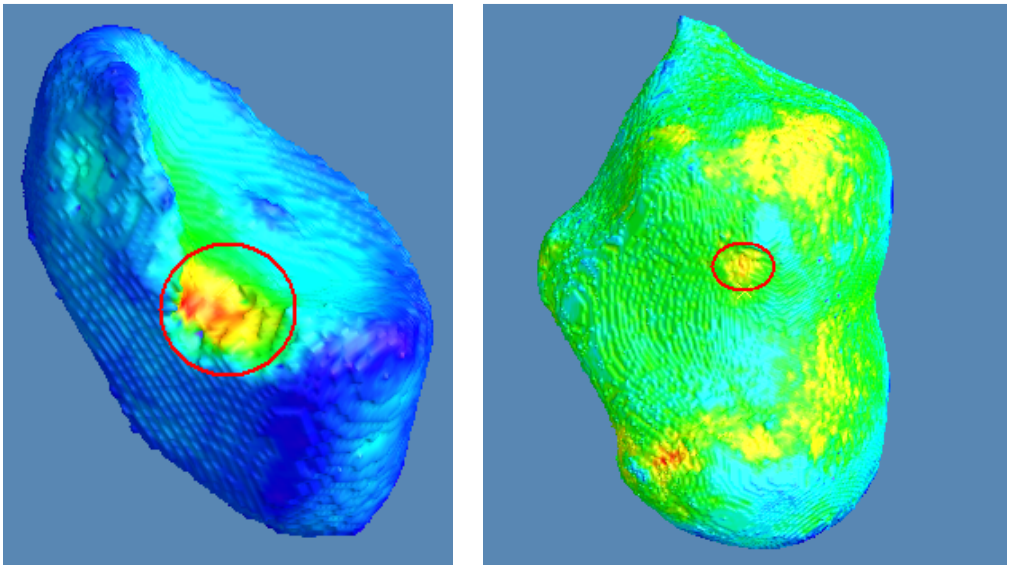

Fig. 4. The 3D display of the inner borders of two cases by viewing from outside the bladders. The superimposed colors indicate the various thickness values resulted from our thickness mapping method. The normalized thickness from 0 to 1 is mapped to purple, blue, cyan, green, yellow, and red. The two red circles in the two images indicate two abnormalities on the bladder wall. Left: a patient bladder with a 3 cm tumor in the red circle. Right: a volunteer bladder without any tumor reported by physicians.

2.4 Conformal mapping

It is well known that the complexity of a 3D problem can be significantly reduced if the problem can be resolved in 2D space. In the study, we employ the conformal mapping algorithm to do the 2D flattening task since it was reported to be the method with minimum distortion and angle preserving [16]. The triangle mesh indicating the inner wall is extracted through using Marching Cube method [17]. The closed mesh is then cut open, so that it is topologically equivalent to a bounded 2D plate. The conformal mapping method is applied to the open mesh, and maps it to a 2D rectangular plate. Fig. 5 shows the resulted 2D image, where the gray level represents the thickness value resulted from the thickness mapping (in Section 2.3). More details of the conformal mapping method are referred to in [18].

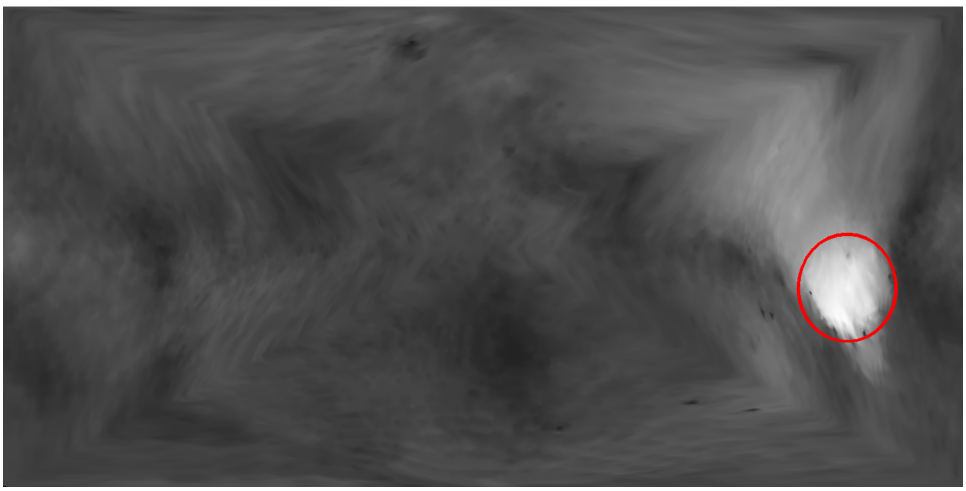

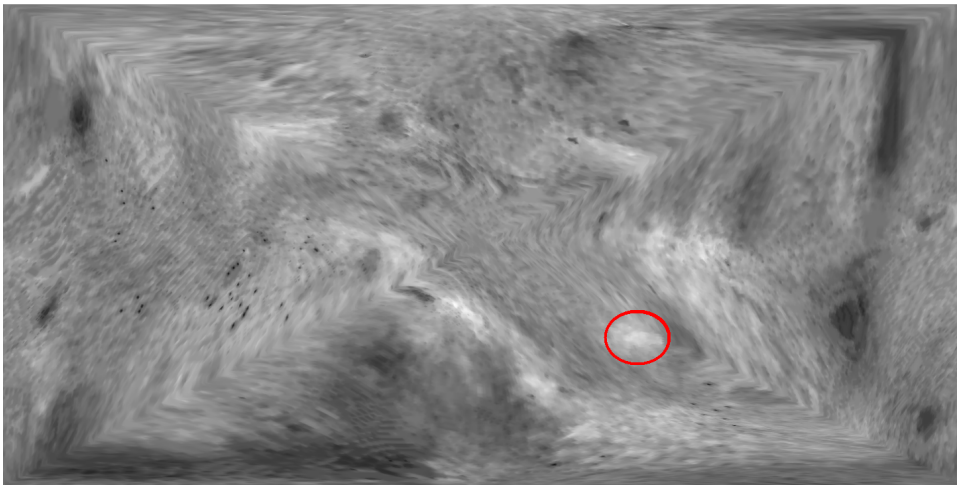

Fig. 5. The flattened 2D display of the two cases shown in Fig. 4, where the gray levels indicate the various thickness. The top and bottom images correspond to the left and right images in Fig. 4, and so does the circled areas.

2.5 Tumor detection

As can be seen in Fig. 4 and 5, the abnormalities are the patches with larger thicknesses, the yellow or red patches in Fig. 4 and highlighted patches in Fig. 5, as compared to their surroundings, the blue or green areas in Fig. 4 and darker areas in Fig. 5. Straightforwardly, those abnormalities can be detected much more easily in 2D space than in 3D space. In the 2D gray images, the abnormalities appear as isolated brighter patches or blobs outstanding their surroundings. Therefore, they can be detected with a 2D blob detector [19], which is based on the Laplacian of the Gaussian (LoG):

$$\nabla^2 L = L_{xx} + L_{yy} \tag{1}$$

where L_{xx} and L_{yy} are the second order derivatives of the convolved image by a Gaussian kernel:

$$L(x, y) = g(x, y, \sigma) \times I(x, y) \tag{2}$$

where g is the Gaussian kernel with scale σ, and I is the flattened 2D image with the texture of thickness mapping. With this method, the LoG gives strong positive responses for dark blobs and strong negative response for bright blobs. In this study, we are only interested in the bright blobs. The scale σ is set to be 3 mm since we only care about lesions larger than 3 mm. Heuristic threshold is applied to the two cases so that pixels with smaller LoG response are labeled and clustered to form the final detections, as shown with the red patches in Fig. 6.

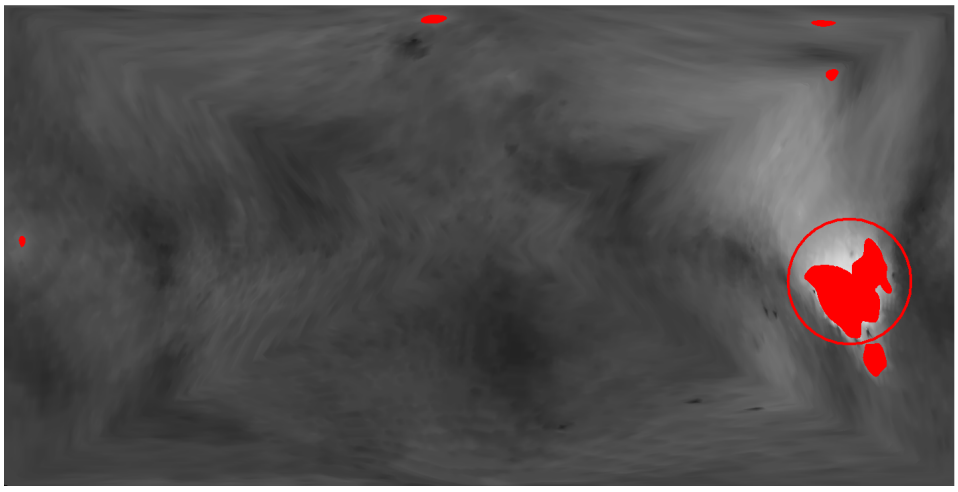

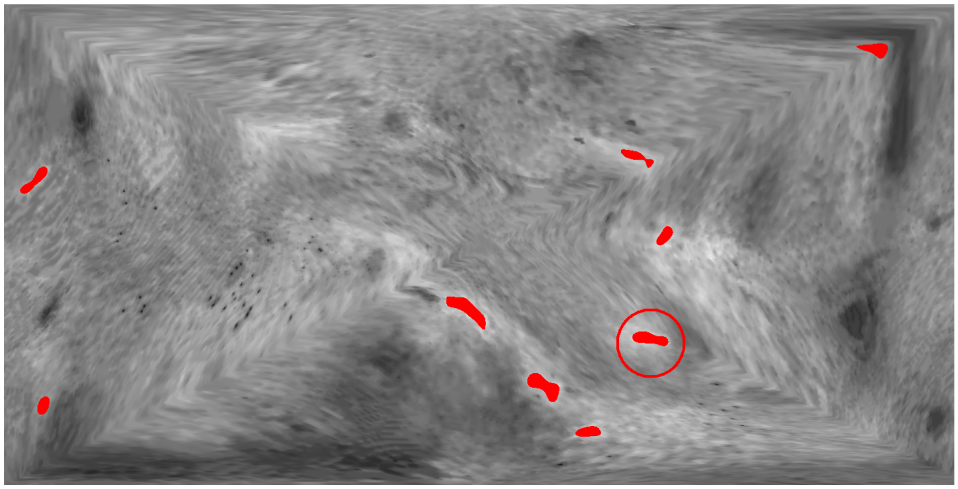

Fig. 6. The detection results on the two cases shown in Fig. 5, indicated by the superimposed red patches from the blob detector with a patch indicating one detection. The two patches in the red circles are actually the same locations as those in the red circles in Fig. 4 and 5.

3 RESULTS

3.1 Data acquisition

Two subjects were recruited under informed consent and IRB approval. One was a patient with a 3 cm tumor reported by physicians. The other was a healthy volunteer without any tumor reported. They were scanned when their bladders were nearly full of urine. A whole body clinical scanner of field strength of 3 Tesla was used with the body coil as the transceiver. A 3D FFE-SPIR CLEAR sequence was applied to acquire the 3D volume data covering the whole bladder. The image datasets have a 2D array size of 256x256 and variable number of slices, depending on the body size. The image voxel size is 0.58 mm in plane and 1.5 mm along the axial direction.

3.2 CAD performance

We applied the above CAD scheme to the two datasets. A total of 15 tumor candidates, as shown in Fig. 6, were generated. After reviewing the original slices by physicians, the two detections indicated by the red circles in Fig. 6 are actually the two objects as shown in Fig. 7. They were the 3 cm tumor, a true positive (TP) detection, and a 4 mm bump caused by severe partial volume, a false positive (FP) detection. The 14 FP detections were mostly due to the image noise, partial volume effect, and other kinds of artifacts like motion artifacts.

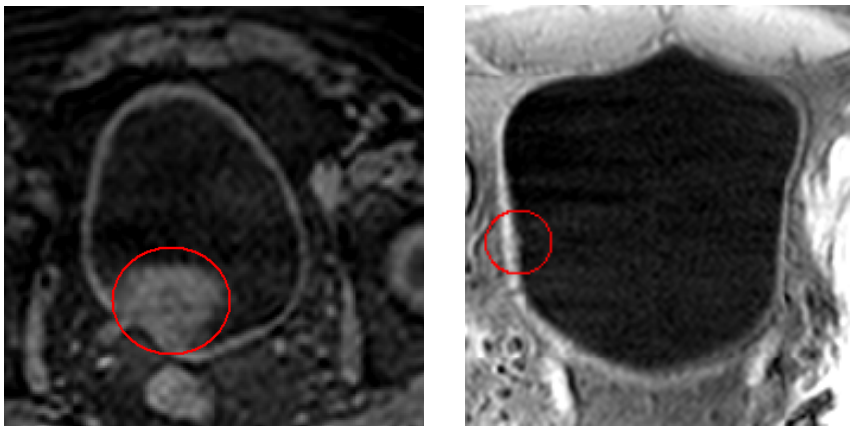

Fig. 7. The original MR transverse slice of the two cases corresponding to those in Fig. 4 near the two circled detections in Fig. 6. Left: the red circle indicates the 3 cm tumor in the patient bladder. Right: the red circle denotes a 4 mm small bump, i.e., an FP detection.

4 DISCUSSION AND CONCLUSION

In this study, we introduced a thickness mapping method based on the segmented bladder wall. In the method, the path used to measure the thickness can be determined without any ambiguity. In the 2D flattened thickness mapping, a blob detector is then applied to detect the abnormalities, which are actually the thickened bladder wall indicating bladder lesions. The method was applied to two study cases and the preliminary result shows 100% detection sensitivity with 7 FPs per case. The whole process is automatically conducted on the computer.

We claimed that our thickness mapping has the ability of exposing sufficient information about small (under 6 mm) or flat lesions for CAD. Unfortunately, there is only one 3 cm tumor in our MR database. Our recruitment is underway and hopefully will acquire more patient studies with smaller tumors. However, the detected 4 mm FP in Fig. 7 implies the potential of our method.

The FP rate is still too high, and the FPs may cost a lot of radiologists' time to confirm that they are not TPs although some of them might be obvious FPs. As future research tasks, we will explore effective features to distinguish TPs and FPs and employ machine learning methods to do classification.

ACKNOWLEDGEMENT

This work was partially supported by NIH Grant #CA082402 and #CA120917 of the National Cancer Institute, NSFC 60628202 and NSF IIS-0713145.

REFERENCES

[1] A. Jemal, A. Thomas, T. Murray, and M. Thun, "Cancer statistics." *A Cancer Journal for Clinicians*, **52**, 23-47, 2002.

[2] S.T. Shaw, S.Y. Poon, and E.T. Wong, "Routine urinalysis: Is the dipstick enough?" *The Journal of the American Medical Association*, **253**, 1596-1600, 1985.

[3] D.L. Lamm and F.M. Torti, "Bladder cancer." *A Cancer Journal for Clinicians*, **46**, 93-112, 1996.

[4] K. Stav, D. Leibovici, E. Goren, A. Livshitz, Y.I. Siegel, A. Lindner, and A. Zisman, "Adverse effects of Cystoscopy and its impact on patients' quality of life and sexual performance." *Isr Med Assoc J.*, **6**, 474-478, 2004.

[5] D.J. Vining, R.J. Zagoria, K. Liu, and D. Stelts, "CT cystoscopy: An innovation in bladder imaging." *American Journal of Roentgenology*, **166**, 409-410, 1996.

[6] Z. Liang, D. Chen, T. Button, H. Li, and W. Huang, "Feasibility studies on extracting bladder wall from MR images for virtual cystoscopy." *Proc. International Society of Magnetic Resonance in Medicine*, **3**, 2204, 1999.

[7] D. Chen, B. Li, W. Huang, and Z. Liang, "A multi-scan MRI-based virtual cystoscopy." *Proc. SPIE Medical Imaging*, **3978**, 146-152, 2000.

[8] M. Lämmle, A. Beer, M. Settles, C. Hannig, H. Schwaibold, and C. Drews, "Reliability of MR imaging-based virtual cystoscopy in the diagnosis of cancer of the urinary bladder." *American Journal of Roentgenology*, **178**, 1483-1488, 2002.

[9] L. Li, Z. Wang, D. Harrington, W. Huang, and Z. Liang, "A mixture-based computed aided detection system for virtual cystoscopy." *Proc. International Society of Magnetic Resonance in Medicine*, **1**, 146, 2003.

[10] S. Jaume, M. Ferrant, B. Macq, L. Hoyte, J.R. Fielding, A. Schreyer, R. Kikinis, and S.K. Warfield, "Tumor detection in the bladder wall with a measurement of abnormal thickness in CT scans." *IEEE Transactions on Biomedical Engineering*, **50**(3), 383-390, 2003.

[11] J.R. Fielding, L. Hoyte, S.A. Okon, A. Schreyer, J. Lee, K.H. Zou, S. Warfield, J.P. Richie, K.R. Loughlin, M.P. O'Leary, C.J. Doyle, and R. Kikinis, "Tumor detection by virtual cystoscopy with color mapping of bladder wall thickness." *The Journal of Urology*, **167**, 559-562, 2002.

[12] Chan T, and Vese L, "Active contours without edges." *IEEE Transactions on Image Processing*, **10**(2), 266-277, 2001.

[13] Duan C, Liang Z, Bao S, Zhu H, Wang S, Zang G and Chen J, "A coupled level set framework for bladder wall segmentation with application to MR Cystography." *IEEE Transaction on Medical Imaging*, 2010, to appear.

[14] Rosenfield A and Pfaltz JL, "Sequential operations in digital picture processing." *Journal of the Association for Computing Machinery*, **13**(4): 471-494. 1966.

[15] Sethian JA: *Level set methods and fast marching methods: evolving interfaces in computational geometry, fluid mechanics, computer vision, and materials science* (2nd ed.). Cambridge University Press, Boston, USA. 1999.

[16] Gu X, Wang Y, Chan T, Thompson P, and Yau S, "Genus zero surface conformal mapping and its application to brain surface mapping." *IEEE Transactions on Medical Imaging*, **23**, 949–958, 2004.

[17] Lorensen WE AND Cline HE, "Marching cubes: A high resolution 3D surface construction algorithm." *Computer Graphics*. **21**(4): 163-169. 1987.

[18] Jiang R, Zhu H, Zeng W, Yu X, Fan Y, Gu X, and Liang Z (2010): "Bladder wall flattening with conformal mapping for MR cystography." *SPIE Medical Imaging 2010*, to appear.

[19] Ballard DH and Brown CM (1982): *Computer Vision*. Prentice Hall, New York, USA.